








## Article

# Optimal Allocation of Renewable Distributed Generators and Electric Vehicles in a Distribution System Using the Political Optimization Algorithm

Nagaraju Dharavat <sup>1</sup>, Suresh Kumar Sudabattula <sup>1</sup>, Suresh Velamuri <sup>2</sup>, Sachin Mishra <sup>1</sup>,  
Naveen Kumar Sharma <sup>3</sup>, Mohit Bajaj <sup>4,5</sup>, Elmazeg Elgamli <sup>6,\*</sup>, Mokhtar Shouran <sup>6</sup> and Salah Kamel <sup>7</sup>

<sup>1</sup> School of Electronics and Electrical Engineering, Lovely Professional University, Phagwara 144411, India

<sup>2</sup> Symbiosis Institute of Technology, Symbiosis International Deemed University, Pune 412115, India

<sup>3</sup> Department of Electrical Engineering, I. K. Gujral Punjab Technical University, Jalandhar 144603, India

<sup>4</sup> Department of Electrical Engineering, Graphic Era (Deemed to be University), Dehradun 248002, India

<sup>5</sup> Department of Electrical and Electronics Engineering, National Institute of Technology, Delhi 110040, India

<sup>6</sup> Wolfson Centre for Magnetics, School of Engineering, Cardiff University, Cardiff CF24 3AA, UK

<sup>7</sup> Electrical Engineering Department, Faculty of Engineering, Aswan University, Aswan 81542, Egypt

\* Correspondence: elgamli@cardiff.ac.uk

**Abstract:** This paper proposes an effective approach to solve renewable distributed generators (RDGs) and electric vehicle charging station (EVCS) allocation problems in the distribution system (DS) to reduce power loss ( $P_{Loss}$ ) and enhance voltage profile. The RDGs considered for this work are solar, wind and fuel cell. The uncertainties related to RDGs are modelled using probability distribution functions (PDF). These sources' best locations and sizes are identified by the voltage stability index (VSI) and political optimization algorithm (POA). Furthermore, EV charging strategies such as the conventional charging method (CCM) and optimized charging method (OCM) are considered to study the method's efficacy. The developed approach is studied on Indian 28 bus DS. Different cases are considered, such as a single DG, multiple DGs and a combination of DGs and EVs. This placement of multiple DGs along with EVs, considering proper scheduling patterns, minimizes  $P_{Loss}$  and considerably improves the voltage profile. Finally, the proposed method is compared with other algorithms, and simulated results show that the POA method produces better results in all aspects.

**Keywords:** microgrid (MG); fuel cell; solar; wind; power loss ( $P_{Loss}$ ); Electric Vehicles (EVs); optimized charging method



**Citation:** Dharavat, N.; Sudabattula, S.K.; Velamuri, S.; Mishra, S.; Sharma, N.K.; Bajaj, M.; Elgamli, E.; Shouran, M.; Kamel, S. Optimal Allocation of Renewable Distributed Generators and Electric Vehicles in a Distribution System Using the Political Optimization Algorithm. *Energies* **2022**, *15*, 6698. <https://doi.org/10.3390/en15186698>

Academic Editor: Philippe Leclère

Received: 24 July 2022

Accepted: 7 September 2022

Published: 13 September 2022

**Publisher's Note:** MDPI stays neutral with regard to jurisdictional claims in published maps and institutional affiliations.



**Copyright:** © 2022 by the authors. Licensee MDPI, Basel, Switzerland. This article is an open access article distributed under the terms and conditions of the Creative Commons Attribution (CC BY) license (<https://creativecommons.org/licenses/by/4.0/>).

## 1. Introduction

The Paris Agreement, signed in 2015 by parties of the United Nations Framework Convention on Climate Change (UNFCCC), was a significant agreement to combat global warming. To meet the aims of this agreement, several countries worldwide foresee a fully carbon-free and sustainable energy grid by 2050 [1]. The use of renewable energy sources (RES) is rapidly increasing to meet expanding global electricity demand. Wind and solar RES presently provide the most worldwide renewables, and they are predicted to continue their phenomenal rise to overtake mainstream power plants in the power generation sector. This rise is primarily due to the environmental benefits of renewable energy over conventional power plants, such as reduced CO<sub>2</sub> pollution and global warming, the economic benefits of RESs and the creation of employment opportunities [2]. The coal-fired power plants are far from the load centres, resulting in significant losses in transmission and distribution (T&D). Distributed Generators (DGs) are small, economical, and decentralized power production systems that rely primarily on renewables such as solar, wind energy, and fuel cells and are situated near load centres. Using RES-based DGs to generate electricity has several advantages, including reduced  $P_{Loss}$ , zero-carbon output, lower operational expenses and enhanced voltage profile.

Furthermore, EV utilization in the current scenario has increased drastically throughout the world. This creates problems in the existing system, particularly during peak demand. However, from an environmental perspective, the use of EVs is vital in the transportation sector. Furthermore, proper assessment is needed in a microgrid (MG), such as integrating DGs and EVs. The concept of an alternative source MG and its control has grown as one of the most important research areas in the electricity sector [3].

“A MICROGRID is defined as a group of Distributed Energy Resources (DERs), including Renewable Energy Sources (RES) and Energy Storage Systems (ESS), plus loads that operate locally as a single controllable entity” [4]. To tackle the stated problem, non-dispatchable DG sources such as solar photo voltaic (PV) and wind turbines (WT), as well as dispatchable DG sources such as fuel cells (FCs) and EVs as load, are included in the MG design.

For generating electricity, proton exchange membrane fuel cells (PEMFC) and solid oxide fuel cells (SOFC) are the most often utilized technologies. Compared to PEMFC, SOFC offers advantages such as waste heat recovery power and high stability, making it ideal for low voltage MG applications. SOFC is particularly cost-effective and ideally suited for poly-generation applications, since it can run at very high temperatures without using a costly platinum catalyst. Due to the uncertain nature of solar and wind power output to weather conditions, PV systems and wind turbines cannot meet the expanding energy demand. As a result, an alternative energy source, such as a fuel cell or energy storage, is necessary. PV systems, wind turbines, and SOFCs are considered DGs in this study, and FC is also employed as a backup source [3,5]. Plug-in electric vehicles (PEVs) are considered dynamic loads during the charging phase and demand electricity from the current grid infrastructure. Adding PEVs to the grid increases losses and decreases the voltage profile when combined with the existing load. As a result, it is essential to investigate the influence of PEVs on the grid.

The MG has two modes of operation: grid connection and self-contained. In grid connection mode, the MG may interchange power with and from the utility while maintaining a constant frequency set by the power system. Self-contained MGs must be able to meet real and reactive power demands with its own inverter-connected DGs. In an MG, the RES-based DGs are intermittent, resulting in various power system challenges. As a result, developing an effective control scheme for controlling DGs is necessary to provide smooth power flows, excellent power supply, and different ancillary services.

Numerous strategies have been proposed in the literature to allocate DGs in distribution networks. In [6], authors presented an intelligent water drop (IWD) method for optimal siting and sizing of DGs into a radial distribution system (RDS) to decrease losses. The meta-heuristic hybrid grey wolf optimization method was implemented for reducing  $P_{Loss}$  and revamping voltage profile in RDS [7]. In [8], this author modified the whale optimization methodology to increase voltage stability and decrease  $P_{Loss}$  in DS for a fixed load demand. This paper proposes a novel improved metaheuristic chaotic search group algorithm (CSGA) to optimally allocate DGs in DS for minimizing active  $P_{Loss}$  [9,10]. The author’s artificial ecosystem optimizer (AEO) method considered studying the optimal allocation of DGs and capacitors in RDS; the objective is shrinking  $P_{Loss}$ .

In [11], this research implemented the particle swarm optimization method for optimal solar and wind DGs location and size in the DS.  $P_{Loss}$  reduction and voltage stability enhancement are considered objective. The proper size, type, and location of renewable DGs in RDS are determined using this study’s mixed-integer conic programming (MICP) model [12,13]. The moth–flame optimization (MFO) algorithm was approached to determine the suitable size and placement of solar and wind DGs in RDS to minimize  $P_{Loss}$  and improve voltage profile and reliability. This study discusses optimal RES-based DGs size and allocation in the RDS. The optimization method CPSO (Constriction Coefficient Particle Swarm Optimization) reduces overall energy loss [14]. The water, energy and food algorithm with suitable allocation and sizing of renewable DGs for power loss reduction in DS was studied [15].

In [16], GA-PSO was used to determine the optimal allocation of renewable-based DGs location size and number, along with an electric vehicle charging station (EVCS) in DS to solve multi-objective voltage and load fluctuation problems. The hierarchical optimization method (HOM) was developed to solve the optimal allocation of solar and wind based-DGs and EVs into DS to decrease  $P_{Loss}$  [17]. This article presents a technique to find the best place to charge EVs in a microgrid. The suggested approach is based on particle swarm optimization (PSO) and optimum power flow (OPF), reducing losses [18]. The proposed methods of differential evolution (DE) and harries hawks optimization (HHO) determine DG sizes; the main objective is to reduce energy losses, system voltage deviation, land cost and  $P_{Loss}$  [19]. The suggested hybrid strategy plans EV and DG scheduling to decrease  $P_{Loss}$  and enhance voltage profile. The research object in this paper is a micro-grid constituted of power distribution such as wind power and photovoltaic (PV), EVCSs, and energy storage systems (ESS). The charging needs of EVs and the output of renewable energy sources are taken into account [20].

In the literature [21–24], most authors determined DG size for a static or fixed demand. However, in practical aspects, the load varies dynamically according to the time. Furthermore, the output power generation of renewable sources is not constant and depends upon environmental changes. So, it is vital to consider the variable load demand and calculate the exact output power from renewable resources. Furthermore, the DGs that produce constant output power are considered as backup devices, along with the renewable DGs. Finally, the authors considered EV integration as an additional load. However, its charging and discharging patterns and their impact on the system are not appropriately addressed. So, in this paper, the authors proposed an effective methodology to solve MG's RDG and EV allocation problems.

Two distinct groups of EVs are determined, and an appropriate rule-based method for charging and discharging the vehicles is presented based on their dominant attributes. Furthermore, the system's loss reduction is addressed by placing DGs and EVs in optimal locations. The selected area will be suitable for any form of DG (solar, wind, or fuel cell) and will be at the utility's decision.

The contribution of this paper is as follows

1. A combined approach such as VSI and POA is proposed to solve RDGs (Solar, Wind and Fuel cell) and EVCS allocation problems in DS. Furthermore, the uncertainties of RDGs, EV charging and discharging patterns are adequately considered.
2. A voltage stability index (VSI) approach is utilized to decide the installation of DGs at weaker nodes and EVs at stronger nodes in the DS.
3. This article determines the appropriate sizes of DGs (solar, wind and fuel cell) for specified load levels using a POA.
4. The EVs are analysed while taking into account the essential aspects, along with the EV state of charge (SoC), travel constraints, EV battery size, and charging/discharging ranges. An optimized charging technique for charging and discharging EVs is offered.

The following are the remaining sections of the article. The system description is discussed in the following Section 2. Presented problem formulation, objective function and mathematical modelling of sources in Section 3. Method of Scheduling for RDGs and EVs in Section 4. Results, discussion and conclusion are given in Sections 5 and 6.

## 2. System Description

Microgrid technology is used to assess the suggested approach's efficacy under diverse circumstances. This case study has three DG units: fuel cells, wind turbines, and solar systems. We considered Solar PV as  $DG_1$ ; wind Turbine as  $DG_2$ , fuel cell as  $DG_3$ , and a backup source of both  $DG_1$  and  $DG_2$  to deal with the erratic nature of wind-solar PV systems. The DGs are linked to loads via dc power interconnections. Electric vehicle charging stations (EVCS) are considered as an additional load. Furthermore, EVs consume electricity from MG during the grid to the vehicle (G 2 V) and also send back electricity to

MG during vehicle 2 grid (V2G). Figure 1 represents autonomous MG. In Table 1 all the specifications of sources are given.

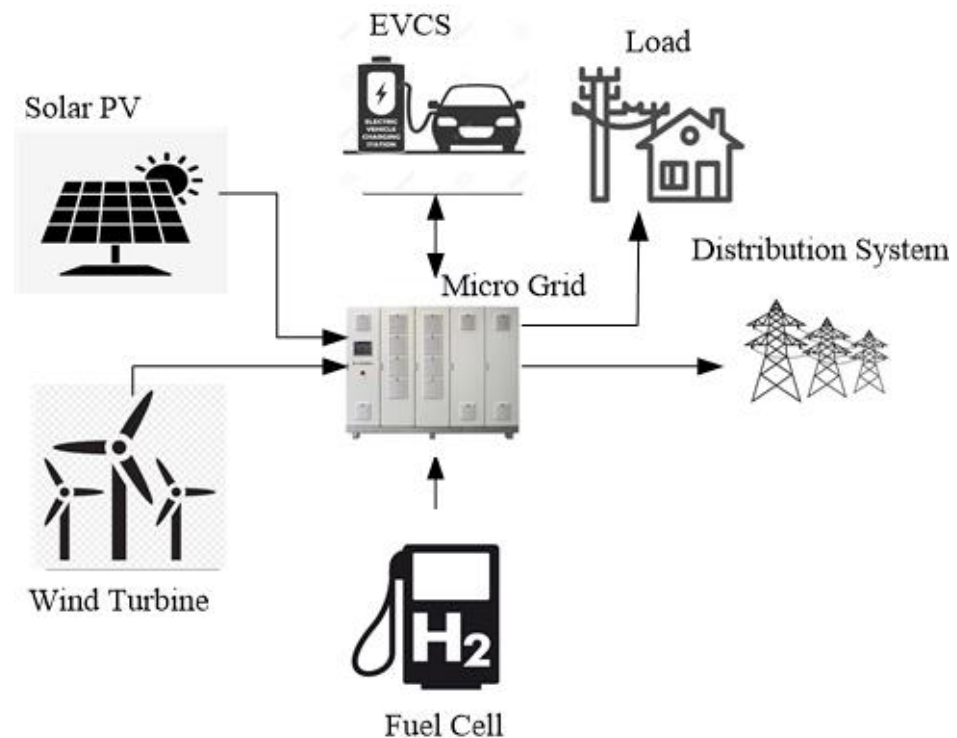


Figure 1. Characteristics of autonomous MG.

Table 1. Specifications of sources.

Description	Specifications	Ratings
Solar PV	Solar panel	220 W
	Ambient Temperature ( $T_a$ )	30.76 °C
	Nominal cell operating temperature ( $N_{ot}$ )	43 °C
	Open Circuit Voltage	36.96 V
	Short Circuit Current	8.38 A
Wind Turbine	Wind Turbine	3000 kW
	Cut-in Speed	3.5 m/s
	Cut-out Speed	25 m/s
	Hub height	66 m
EVs	Rated Speed	15 m/s
	E.V Capacity or Battery	16 kWh
	No. of EVs	60
	$SoC_{min}$	0.2
	$SoC_{max}$	0.9
	Avg. power consumption per km	0.175 kWh/km
	Avg. distance travelled by each EV	30 km

### 3. Problem Formulation

The proposed method's primary objective is to allocate DGs (solar, wind and fuel cell) and EVs in the DS in the most effective way to reduce  $P_{Loss}$  and improve voltage profile.

#### 3.1. Objective Function

The objective  $P_{Loss}$  reduction is

$$\min \sum_{n=1}^{24} P_{loss}(n) \quad (1)$$

where

$$P_{Loss}(n) = \sum_{n=1}^{24} I_n^2 R_n \tag{2}$$

The following are the main constraints related to the objective function  
 Power balance constraints:

$$\sum_{n=1}^{24} P^{SDG}(n) + \sum_{n=1}^{24} P^{WDG}(n) + \sum_{n=1}^{24} P^{SOFC_{DG}}(n) = \sum_{n=1}^{24} [P^{Demand}(n) \pm P^{EV}(n) + P_{Loss}(n)] \tag{3}$$

where,  $P^G(n)$  =  $n$ th hour power generator,  $P^{Demand}(n)$  =  $n$ th hour power demand,  $P^{EV}(n)$  = during an  $n$ th hour, EV supplied/consumed power.

Bus Voltage Profile Constraints:

DS's voltage profile must always be within the specified ranges.

$$V_{k,n}^{min} \leq V_{k,n} \leq V_{k,n}^{max} \tag{4}$$

where,  $V_{k,n}$  =  $k$ th bus voltage at the  $n$ th hour.

DS's voltage profile must always be within the specified ranges.

This section given information about modelling various resources with equations.

### 3.2. Modelling of Sources

This work utilises and allocates solar, wind and fuel cell-based DGs in the DS. The system injected solar, wind and fuel cell-based DGs that activate power and analysed the unity power factor. Before assigning DG into DS, we need to consider generation uncertainties associated with solar, wind and fuel cell DGs and determine the output power.

#### 3.2.1. Mathematical Modelling of Fuel Cell

FC will strive to satisfy the remaining load when solar and wind power is inadequate to meet the load in a hybrid energy system. For electricity generation, FC requires hydrogen. A fuel cell's power output can be calculated mathematically, as represented in Equations (5) and (6) [21,22].

$$P^{FC} = E^{FC_0} * I^{FC} - \frac{R^{FC} * (I^{FC})^2}{A^{FC}} \tag{5}$$

Here,  $E^{FC_0}$  = Potential difference

$I^{FC}$  = current flow

$R^{FC}$  = FC electrodes have an internal resistance between them

$A^{FC}$  = FC electrode surface area

$$V^{FC} = N^0 \left( E^0 + \frac{RT}{2F} \log \left( \frac{p_{H_2} p_{O_2}^{0.5}}{p_{H_2O}} \right) \right) - r I^{LFC} \tag{6}$$

$R, r$  = global gas constant (J/mol k), internal resistance (ohm)

$T$  = Temperature (kelvin)

$p_{H_2}, p_{O_2}, p_{H_2O}$  = hydrogen, oxygen and water (atm)

$N^0, E^0$  = No. of Cells, reversible cell (volts)

#### 3.2.2. Mathematical Modelling of Solar Irradiance

Solar panel exact output power calculated with beta probability distribution function (PDF). Beta PDF is more suitable for statistical analysis to model solar irradiance [11]. Figure 2 represents expected output power from solar module.

$$f_s^m(s) = \frac{\Gamma(\alpha^m + \beta^m)}{\Gamma(\alpha^m) \cdot \Gamma(\beta^m)} \cdot (s^m)^{\alpha^m - 1} \cdot (1 - s^m)^{\beta^m - 1} \text{ For } \alpha^m > 0; \beta^m > 0 \tag{7}$$

$m, \Gamma$  = Gamma function.

With mean ( $\mu$ ), Standard deviation ( $\sigma$ ) determined  $f_s^m(s), s = \frac{kW}{m^2}$

$$\beta^m = (1 - \mu_s^m) \cdot \left( \frac{\mu_s^m (1 + \mu_s^m)}{(\sigma_s^m)^2} - 1 \right) \tag{8}$$

$$\alpha^m = \frac{\mu_s^m * \beta^m}{(1 - \mu_s^m)} \tag{9}$$

$\alpha^m, \beta^m$  = Shape parameters.

$$P^{PVA}(s) = N^{PVM} * V^y * I^y * FF \tag{10}$$

where

$$FF = \frac{V^{MPP} * I^{MPP}}{V_{oc} * I_{sc}} \tag{11}$$

$$I^y = s \left[ I_{sc} + K^i (T^{cy} - 25) \right] \tag{12}$$

$$V^y = V_{oc} - K^v * T^{cy} \tag{13}$$

$$T^{cy} = T^A + s \left( \frac{N^{OT} - 20}{0.8} \right) \tag{14}$$

FF = fill factor, the sum of all PV modules =  $N^{PVM}$ ,  $I_{sc}$  = short circuit current,  $V_{oc}$  = open-circuit voltage,  $T^{cy}$  = cell temperature,  $T^A$  = ambient temperature,  $K^i, K^v$  = current and voltage temperature coefficients,  $N^{OT}$  = nominal operating temperature.

$$P(s) = P^{PVA}(s) * f_s^m(s) \tag{15}$$

$$\text{Total Expected Output Power} = \int_0^1 P^{PVA}(s) * f_s^m(s) \tag{16}$$

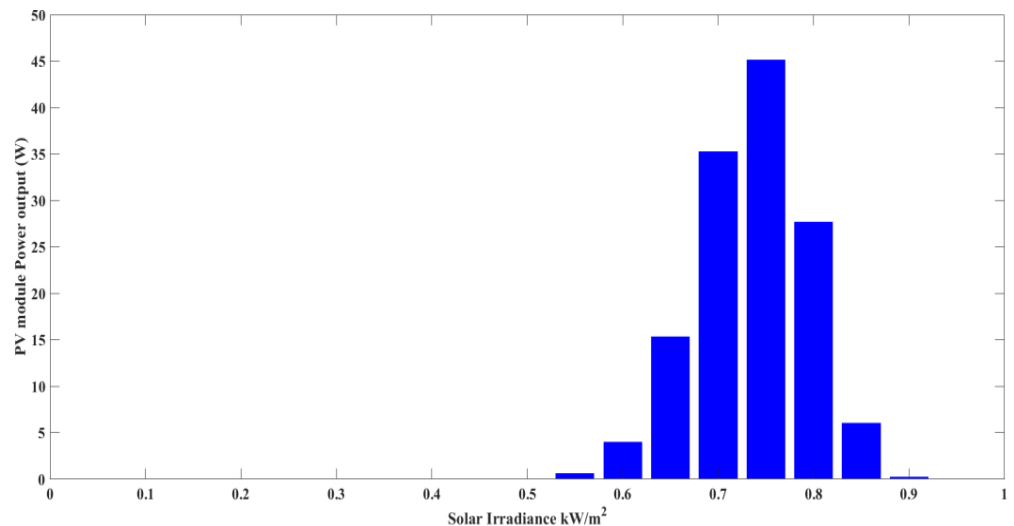


Figure 2. Expected Output Power from Solar Module.

### 3.2.3. Mathematical Modelling of Wind Speed

The wind speed significantly impacts the output power of wind-based DGs. Therefore, the uncertainty related to wind speed is adequately simulated before placing these sources in DS. Weibull PDF has been utilized for these [11]. Figure 3 represents Wind turbine expected output power for 1 h.

$$f_v(V) = \frac{k}{c} \cdot \left( \frac{v}{c} \right)^{k-1} \cdot e^{-\left( \frac{v}{c} \right)^k} \text{ for } c > 1; k > 0 \tag{17}$$

where,  
 k = shape factor, c = scale factor

$$k = \left(\frac{\sigma}{\mu}\right)^{-1.086} \tag{18}$$

$$c = \frac{\mu}{\Gamma\left(1 + \frac{1}{k}\right)} \tag{19}$$

$$P_{WT}(V) = \begin{cases} 0 & \text{for } 0 \leq v < v_{cut-in} \text{ and } v > v_{cut-out} \\ a \cdot v^3 + b \cdot P_r & \text{for } v_{cut-in} \leq v \leq v_r \\ P_r & \text{for } v_r \leq v \leq v_{cut-out} \end{cases} \tag{20}$$

where

$$a = \frac{P_r}{\left(v_r^3 - v_{cut-in}^3\right)} \tag{21}$$

$$b = \frac{P_r}{\left(v_r^3 - v_{cut-in}^3\right)} \tag{22}$$

$$P_{WE} = P_{WT}(V) * f_v(V) \tag{23}$$

$$\text{Expected total output power} = \int_0^1 P_{WT}(V) * f_v(V) dv \tag{24}$$

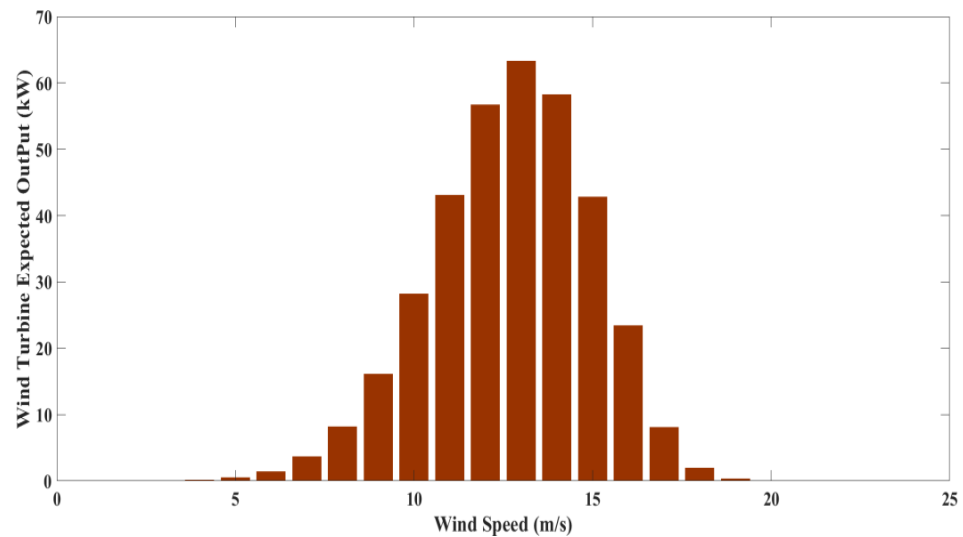


Figure 3. Wind turbine expected output power for 1 h.

### 3.2.4. Mathematical Modelling of EV Uncertainty

Users determine when to charge (DoC), depending on the charging SoC, trip distance and charge power. The DoC is influenced by the following trip’s distance among these variables.

The primary SoC of *m*th EV at *n*th hour below equation

$$SoC_n^m = \left(1 - \frac{\tau t}{t_r}\right) \cdot 100\% \tag{25}$$

where  $\tau$  = no. of trips,  $t$  = EV travel distance,  $t_r$  = EV travel range

Battery Storage Constraint:

$$SoC_{min} \leq SoC_n^{EV} \leq SoC_{max} \tag{26}$$

$$P_{ch, n, t} \leq P_{ch, n}^{max} \quad (27)$$

$$P_{disch, n, t} \leq P_{disch, n}^{max} \quad (28)$$

#### 4. Method for Scheduling of RDGs & EVs

##### 4.1. Conventional and Optimized Charging Methods for EVs

After arriving home in the conventional charging method (CCM), the EVs are instantly connected to a charging point. They are unconcerned with the demands of the system. The traditional charging approach may not be advantageous because it results in significant energy loss, a system voltage decrease, and system maloperation caused by congestion. The suggested technique should help charge EVs (V 2 G) during off-hours and transfer electricity to the grid (G 2 V) during peak hours. EV charging and discharging are prioritized based on demand. This strategy is referred to as the optimized charging method. In this strategy, EV consumers care about system load. EVs are not allowed to be charged during peak load. EVs are charged during low-load hours through an optimized charging method, following the load demand curve. A consistent voltage profile and low  $P_{Loss}$  are obtained using an optimized charging method. Using this approach, the utility and EV consumers will communicate about the system's demand and devise new strategies for enhancing the system's efficiency. Scheduling is based on the system's peak-to-average ratio (PAR) of demand. Figure 4 represents Flow chart steps for Scheduling EVs.

The fundamental aim of EV scheduling is to reduce PAR, as shown:

$$PAR = \frac{P_{d, peak}}{P_{d, mean}} \quad (29)$$

where  $P_{d, mean}$  = average system demand,  $P_{d, peak}$  = peak system demand

This work provides a suitable scheduling technique to reduce the PAR.

Charge or discharge is also determined by the power ratio ( $P_R$ ) magnitude, which is represented as follows:

$$P_R = \frac{P_D(n)}{P_{d, mean}} \quad (30)$$

It is essential to keep two conditions in mind: the number of EVs assigned should not be minus, and the amount of EVs granted at the next step must be larger than the number in the first step.

$$\sum_{t=1}^N EV_{pit} \leq EV_T \quad (31)$$

Scheduling procedures to follow.

- The optimized charging method first looks at the type of vehicle, how many vehicles need to be charged, how much each vehicle needs to be charged, and how long the system will run before the next trip.
- For each hour, the PAR and power ratio is calculated with or without taking EVs into account.
- (V2G) mode is started if the power ratio ( $P_R$ ) is smaller than the average power demand  $P_{d, mean}$ .
- If the  $P_R$  of the specific interval time is larger than the overall power demand  $P_{d, mean}$ , the vehicle can send electricity back to the grid while taking into account the existing SoC.
- These details will be sent to the POA method every hour to identify the optimal size of renewable DGs.
- Once the EVs have reached SoC and are available for the next journey, the procedure is completed.



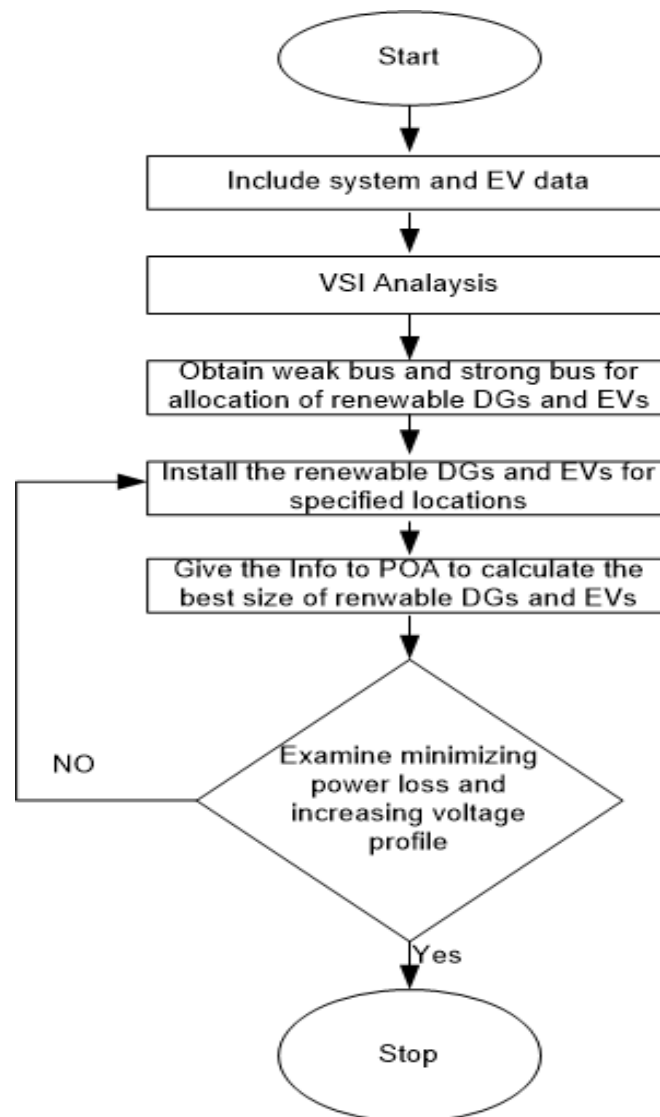


**Figure 4.** Flow chart steps for Scheduling EVs.

#### 4.2. Best Placement of RDGs and EVCSs Using VSI

“By using this voltage stability index, one can measure the level of stability of radial distribution networks and thereby appropriate action may be taken if the index indicates a poor level of stability” [23]. With VSI on each bus, the suitable location of RDGs and EVCS can be found. This approach takes into account the total system load demand for each hour and chooses the best placement. VSI is utilized in this paper with some modifications for finding desired locations [23]. A comprehensive analysis of VSI can be determined by Equation (32). All buses are rated and evaluated on the obtained value of VSI, a bus is regarded as stronger if the value of VSI is close to 1 and bus is considered weak if the estimated value is close to 0. This technique selects the stronger buses for EVCS placement, while the weaker buses are evaluated for RDGs placement. In this manner, the suitable locations for renewable DGs and EVCS are being considered. Figure 5 represents procedure for placement of renewable DGs and EVs with VSI.

$$VSI = 2V_s^2 V_r^2 - V_r^4 - 2V_r^2 (PR + QX) - (P^2 + Q^2) |Z|^2 \quad (32)$$

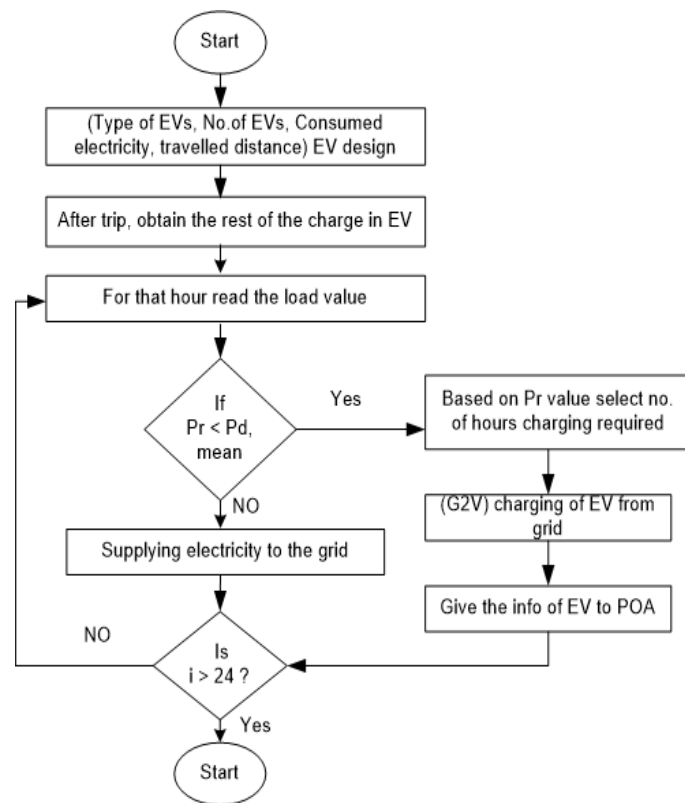


Figure 5. Procedure for placement of renewable DGs and EVs with VSI.

4.3. Renewable DGs and EVs Sizing Finding with Political Optimizer Algorithm (POA)

Askari introduced a unique universal optimisation meta-heuristic called Political Optimizer (POA). It is a human behaviour-based application influenced by a multi-step western political environment. This technique can resolve traditional mathematical design issues, extraordinary convergence speed in data analysis, and fast iterations. “PO consists of five stages 1. Party formation, 2. Constituency allocation, 3. Election campaign, 4. Party switching, 5. Parliamentary affairs” [24–26]. Figure 6 represents POA multiple-step Process.

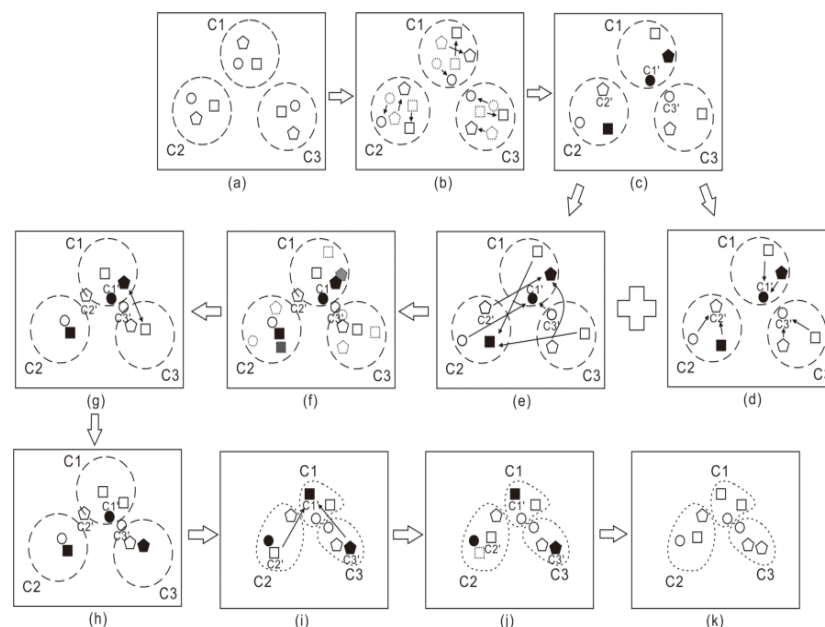


Figure 6. POA multiple-step process [26].

Total population categorised into  $n$  political parties is shown in the below equations:

$$P = \{P_1, P_2, P_3, \dots, P_n\} \tag{33}$$

Every single party contains  $n$  party associates

$$P_i = \{P_i^1, P_i^2, P_i^3, \dots, P_i^n\} \tag{34}$$

Every party associate considers dimension  $d$

$$P_i^j = [P_{i,1}^j, P_{i,2}^j, P_{i,3}^j, \dots, P_{i,d}^j]^T \tag{35}$$

Represented electoral districts  $n$  below equation

$$C = \{C_1, C_2, C_3, \dots, C_n\} \tag{36}$$

Assumed every constituency consisted of  $n$  associates

$$C_j = \{P_1^j, P_2^j, P_3^j, \dots, P_n^j\} \tag{37}$$

The leader of the party is represented as an associate with good fitness in the party

$$q = \underset{1 \leq j \leq n}{\operatorname{argmin}} f(P_i^j), \forall i \in \{1, \dots, n\} \tag{38}$$

$$P_i^* = P_i^q$$

Entire leader of the party shown in the below equation

$$P^* = \{P_1^*, P_2^*, P_3^*, \dots, P_n^*\} \tag{39}$$

Victor of every individual constituency is an associate of parliament

$$C^* = \{c_1^*, c_2^*, c_3^*, \dots, c_n^*\} \tag{40}$$

Below equations represent workers to update the election campaign

$$P_{i,k}^j(t+1) = \begin{cases} \text{if } P_{i,k}^j(t-1) \leq P_{i,k}^j(t) \leq m^* \text{ or } P_{i,k}^j(t-1) \geq P_{i,k}^j(t) \geq m^*, \\ \quad m^* + r(m^* - P_{i,k}^j(t)); \\ \text{if } P_{i,k}^j(t-1) \leq m^* \leq P_{i,k}^j(t) \text{ or } P_{i,k}^j(t-1) \geq m^* \geq P_{i,k}^j(t), \\ \quad m^* + (2r-1)|m^* - P_{i,k}^j(t)|; \\ \text{if } m^* \leq P_{i,k}^j(t-1) \leq P_{i,k}^j(t) \text{ or } m^* \geq P_{i,k}^j(t-1) \geq P_{i,k}^j(t), \\ \quad m^* + (2r-1)|m^* - P_{i,k}^j(t-1)|; \end{cases} \tag{41}$$

$$P_{i,k}^j(t+1) = \begin{cases} \text{if } P_{i,k}^j(t-1) \leq P_{i,k}^j(t) \leq m^* \text{ or } P_{i,k}^j(t-1) \geq P_{i,k}^j(t) \geq m^*, \\ \quad m^* + (2r-1)|m^* - P_{i,k}^j(t)|; \\ \text{if } P_{i,k}^j(t-1) \leq m^* \leq P_{i,k}^j(t) \text{ or } P_{i,k}^j(t-1) \geq m^* \geq P_{i,k}^j(t), \\ \quad P_{i,k}^j(t-1) + r(P_{i,k}^j(t) - P_{i,k}^j(t-1)); \\ \text{if } m^* \leq P_{i,k}^j(t-1) \leq P_{i,k}^j(t) \text{ or } m^* \geq P_{i,k}^j(t-1) \geq P_{i,k}^j(t), \\ \quad m^* + (2r-1)|m^* - P_{i,k}^j(t-1)|; \end{cases} \tag{42}$$

$\lambda$  Make use of adaptive parameters and minimise 1 to 0 at the iterative process. Every associate member determined with probability  $\lambda$  and announced the champion of the constituency.

$$q = \underset{1 \leq j \leq n}{\operatorname{argmax}} f(P_i^j) \tag{43}$$

Finally, the election process victor of the constituency is calculated with the below Equation (44).

$$q = \underset{1 \leq j \leq n}{\operatorname{argmax}} f(P_i^j) \tag{44}$$

$$c_j^* = p_q^j$$

Steps to obtain suitable sizes of RDGs using POA and respective flow chart is given in Figure 7.

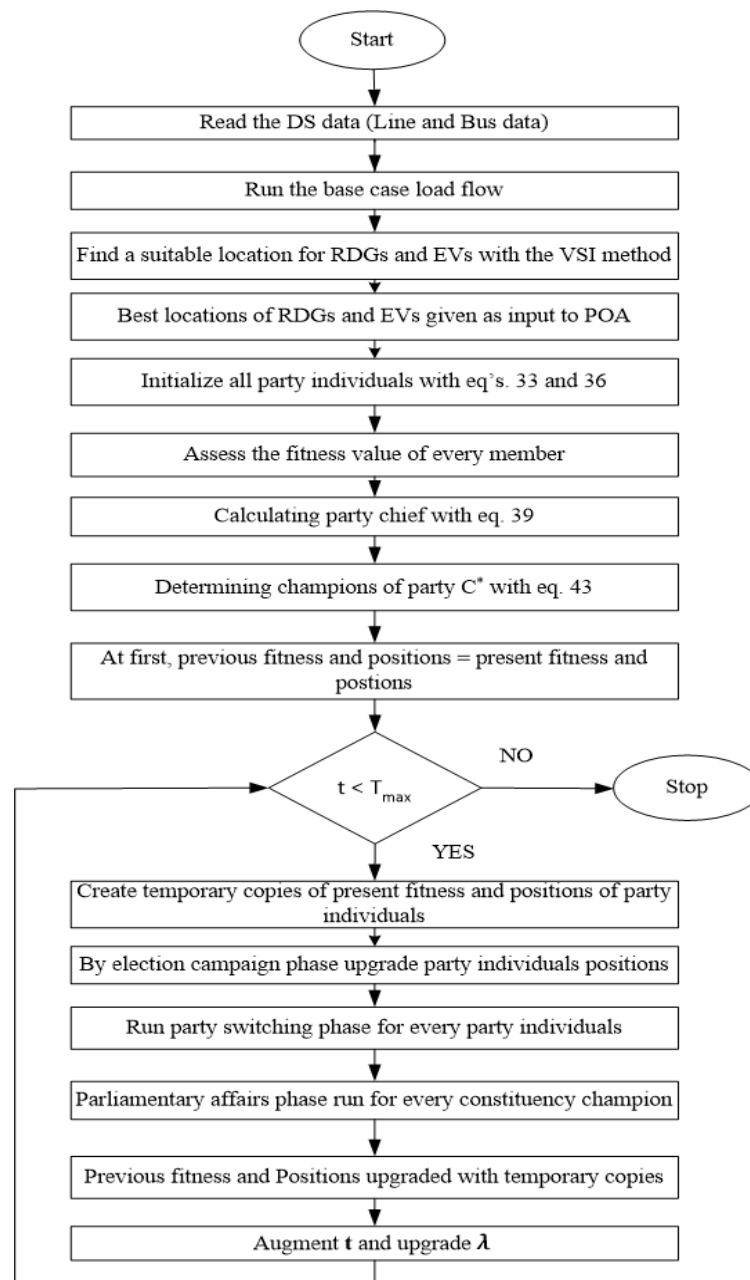
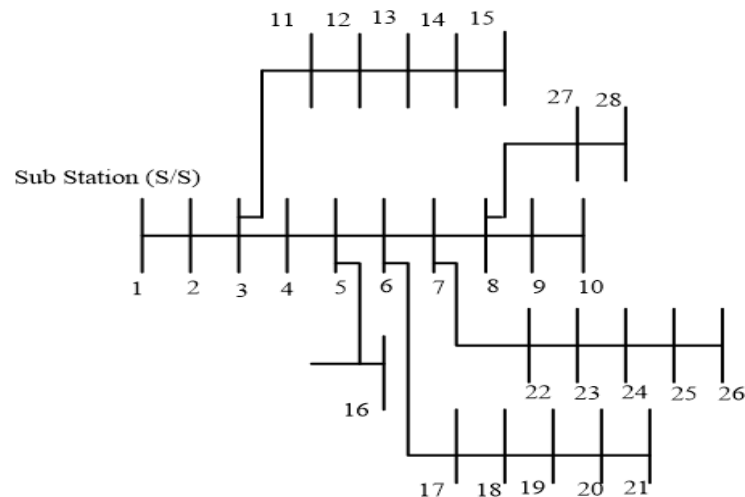


Figure 7. Flow Chart of POA.

- Step 1: Read the line and bus data of DS  
 Step 2: Run the base case load flow  
 Step 3: Find a suitable location for RDGs with the VSI technique  
 Step 4: Determine the suitable installation of RDGs using VSI, the information shared with POA  
 Step 5: According to Equation (33), all residents are divided into 'n' political parties, and each and every party has 'n' members.  
 Step 6: Equation (38) determines the party's leader, while Equation (39) determines each constituency's representative.  
 Step 7: Compare current values to position values from the past  
 Step 8: Establish temporary fitness values and placements at the start of algorithm loops.  
 Step 9: Equations (41) and (42) reflect the second phase of the election campaign, and all political party members' values and views are updated using these EQs.  
 Step 10: Each candidate in the switching phase runs individually in Equation (43), which depicts the election campaign following the phase.  
 Step 11: Constituency champs are determined using Equation (44).  
 Step 12: The algorithm displays all parliamentary location champions in this phase, also known as the period of parliament affairs.  
 Step 13: Upgrade all fitness values ( $P_{Loss}$ ) and placements, such as the finest RDGs, is the last phase.

## 5. Results and Discussion

The influence of RDGs and EVs on the MG is studied by addressing different operating cases, and the results are given in this section. A novel technique for  $P_{Loss}$  reduction and augmenting voltage profile in an MG in the presence of solar wind and fuel cell-based RDGs and various types of EV groups with unique operating patterns are adopted to address the optimisation issue. This strategy combines the proposed optimized EV charging technology with the POA. The 28 Indian real test system were used throughout the study and single line diagram is shown in Figure 8.



**Figure 8.** 28 Indian real test system single line diagram.

Initially, the proposed approach was applied and tested for various cases, such as the location of one DG, two DGs, and three DGs. Table 2 summarizes the findings. According to the findings, the placement of 3 DGs resulted in minimal  $P_{Loss}$ , an enhancement in voltage profile, and an increase in VSI. Due to system capacity and load constraints, going above 3 DGs for the proposed DS is not possible. The system's performance will suffer if the number of DGs is increased above 3. Figure 9 represent the power demand curve. Figure 10 shows that compared to all other cases, 3 DGs reduced 51.10% of  $P_{Loss}$ .

**Table 2.** Results for 28 Indian Real Test System considering different cases.

Different Cases	Bus. No	DG Size (kW)	$P_{Loss}$ (kW)	$V_{min}$ (p.u)	$VSI_{min}$ (p.u)	% Red of $P_{Loss}$
Base Case	NA	NA	68.8189	0.9123	0.6927	NA
1-DG	7	583.0954	37.0066	0.9615	0.8545	46.22
2-DGs	9	403.2352	35.8397	0.9572	0.8395	47.92
	12	272.0916				
3-DGs	7	334.2644	33.6501	0.9633	0.8611	51.10
	12	230.5484				
	22	145.6193				

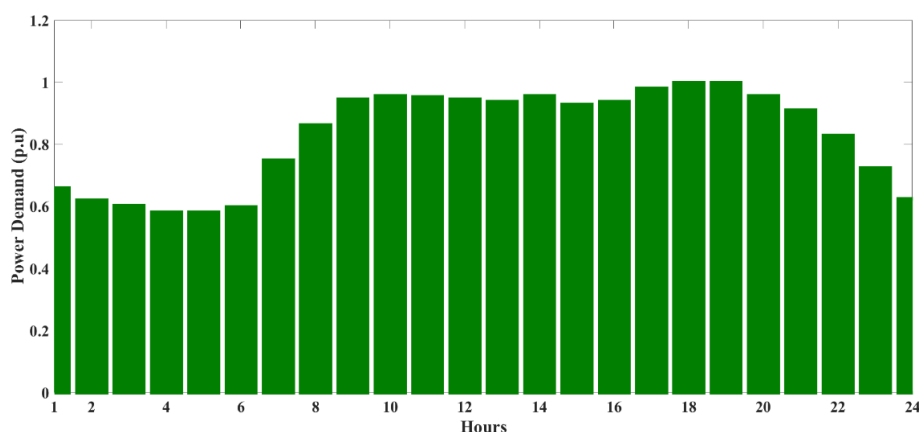


**Figure 9.** System power demand for 24 h.

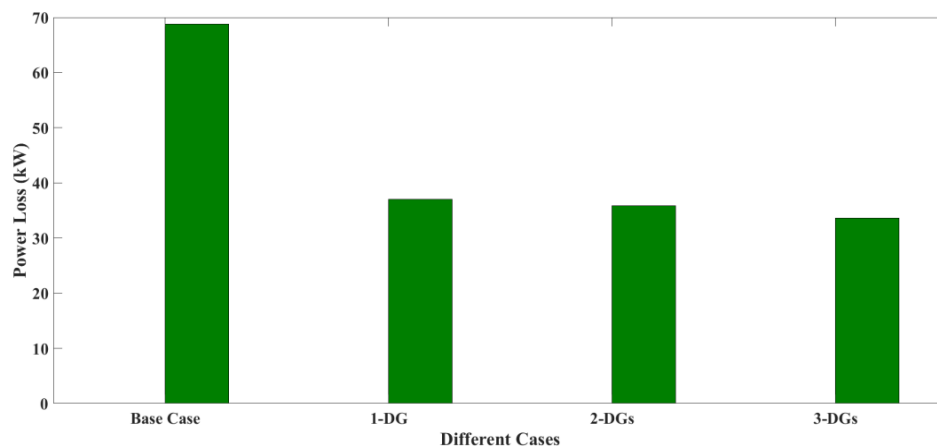


**Figure 10.**  $P_{Loss}$  reduction for different Cases.

To test the effectiveness of the suggested technique, we assessed different load levels, such as half (0.5 p.u), full (1.0 p.u.) and heavy (1.1 p.u.). If the DGs were placed in proper places and of a suitable size at all load levels, energy loss was significantly reduced and voltage profile and VSI were enhanced. Table 3 shows the calculated  $P_{Loss}$ , VSI and voltage profile at various load conditions.

Furthermore, the proposed POA was compared in terms of several criteria to other current optimization approaches such as grasshopper optimization (GOA), whale optimization (WOA), and dragonfly algorithm (DA). The findings of all optimization methods are shown in Table 4 with 50 trials. The  $P_{Loss}$  reduction achieved by POA surpassed all other techniques. The suggested POA has a better standard deviation than all other approaches, indicating its dominance over existing methods.

**Table 3.** Suitable capacity of DGs at different load levels.

Different Loads	Without DG P <sub>Loss</sub> (kW)	With DG P <sub>Loss</sub> (kW)	DG Size in kW	V <sub>min</sub> (p.u)	VSI <sub>min</sub> (p.u)	% Red of P <sub>Loss</sub>
Half Load (0.5)	15.8508	8.132	162.8245 111.5187 72.5212	0.982	0.9299	48.6965
Full Load (1.0)	68.8189	33.6501	334.2578 230.5428 145.6313	0.9633	0.8611	51.1086
Heavy Load (1.1)	84.7675	41.0029	369.6675 255.3580 160.3221	0.9595	0.8475	51.6289

**Table 4.** POA method results compared with other optimisation methods.

Different Methods	DG Size (kW)	P <sub>Loss</sub> (kW)	V <sub>min</sub> (p.u)	VSI <sub>min</sub> (p.u)	Time (s)
GOA	334.5567 230.4150 145.4057 182.5131	33.6501	0.9639	0.8615	13.7916
WOA	262.1375 265.0773 332.81	33.9388	0.9614	0.8542	13.6241
DA	235.1821 145.1592 222.0523	33.6513	0.9634	0.8612	13.7491
POA	220.5258 256.781	32.1337	0.9633	0.8611	13.5817

Tables 4 and 5 show the DG sizes, P<sub>Loss</sub>, and voltage profiles derived using different methods with identical simulation conditions. POA delivers the best outcomes in all aspects compared to other techniques. POA is particularly efficient in producing better results in fewer iterations, with less P<sub>Loss</sub>, voltage profile and voltage stability enhancement, as shown in Figures 11 and 12. As a result, this POA is implemented throughout the research study as an appropriate optimization method. Figure 13, depicts the convergence curves for several optimizer approaches for the given objective function.

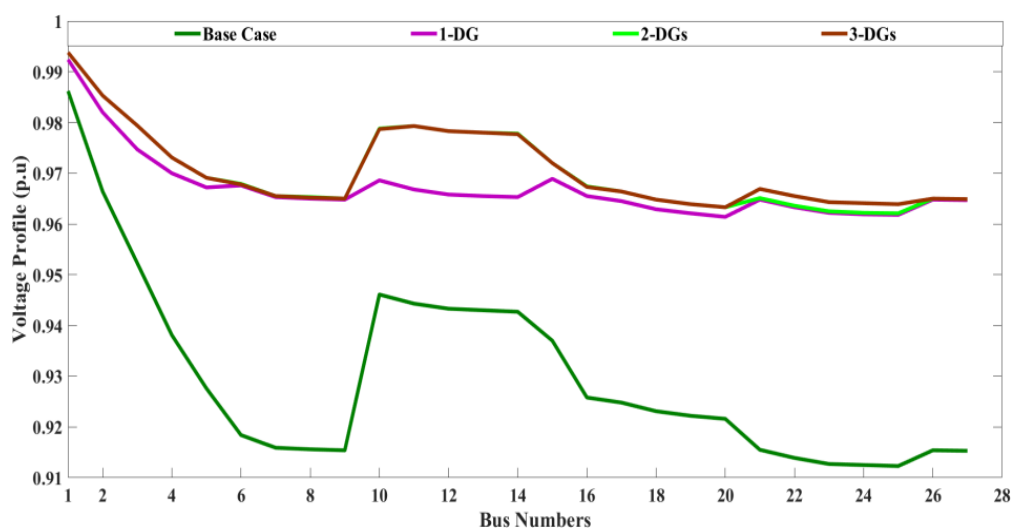


**Figure 11.** Voltage Profile for 28 Test System.

**Table 5.** DG sizes under dynamic load profile without considering uncertainties.

Hours	DG <sub>1</sub> (kW)	DG <sub>2</sub> (kW)	DG <sub>3</sub> (kW)
1	217.0467	148.979	95.977
2	203.4865	139.5917	90.1536
3	197.7144	135.6158	87.6951
4	190.3307	130.4985	84.4631
5	190.3452	130.4988	84.455
6	196.3892	134.681	87.1098
7	247.3955	170.0333	108.9991
8	286.7203	197.383	125.6688
9	315.2901	217.3105	137.6994
10	319.1438	219.9935	139.3215
11	318.0901	219.2612	138.8779
12	315.3042	217.3044	137.6907
13	312.8509	215.5912	136.6694
14	319.1481	219.987	139.3158
15	309.3421	213.1604	135.2089
16	312.8398	215.5972	136.6844
17	327.9367	226.1077	142.9729
18	334.2414	230.5464	145.6437
19	334.2334	230.5656	145.6326
20	319.1343	219.9909	139.3344
21	303.0699	208.7601	132.5754
22	274.6099	188.9348	120.549
23	238.8566	164.0718	105.333
24	204.8351	140.523	90.7436

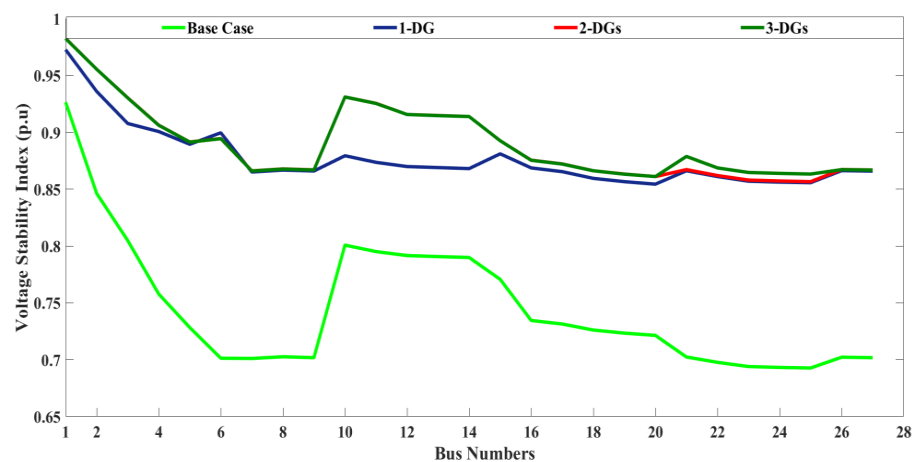


**Figure 12.** Voltage Stability Index for 28 Test System.

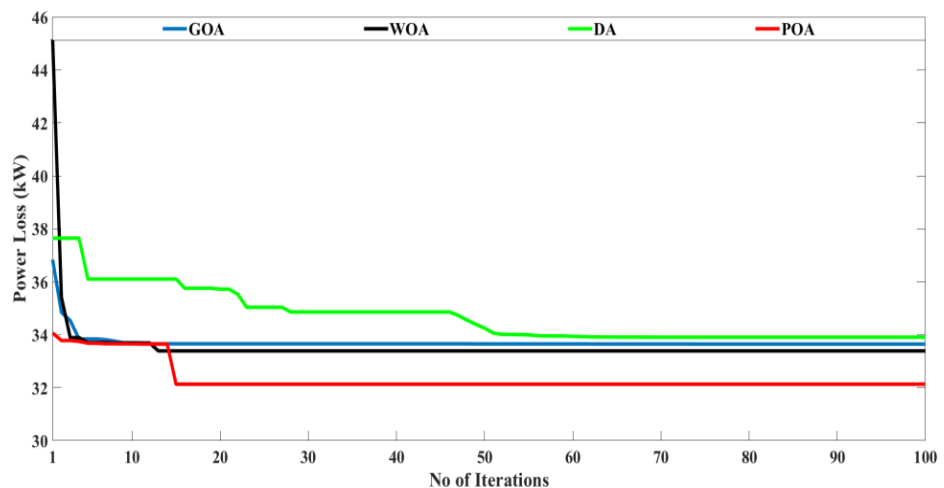


**Figure 13.** POA Comparisons with Other methods.



### 5.1. 28 Indian Real Test System Evaluation without EVs

The VSI approach allocates DGs to the 7th, 12th, and 22nd buses. Table 5 shows the results of POA optimization in deciding the suitable DG size for time-varying load conditions without considering the generation uncertainties of DGs. After installing the DGs, the  $P_{Loss}$ ,  $V_{min}$ , and  $VSI_{min}$  at each and every hour are determined, and the outcomes are compared to the initial case. Figure 10 depicts the variation in  $P_{Loss}$  achieved before and after DG placement. Compared to the initial case study, there was a considerable decrease in overall  $P_{Loss}$ . Figures 11, 12, 14 and 15 also show the difference in  $V_{min}$  and  $VSI_{min}$  before and after introducing DGs. Compared to the base case, there was an enormous improvement in voltage profile and VSI. This demonstrates POA's effectiveness in allocating the appropriate DG size based on the load demand.

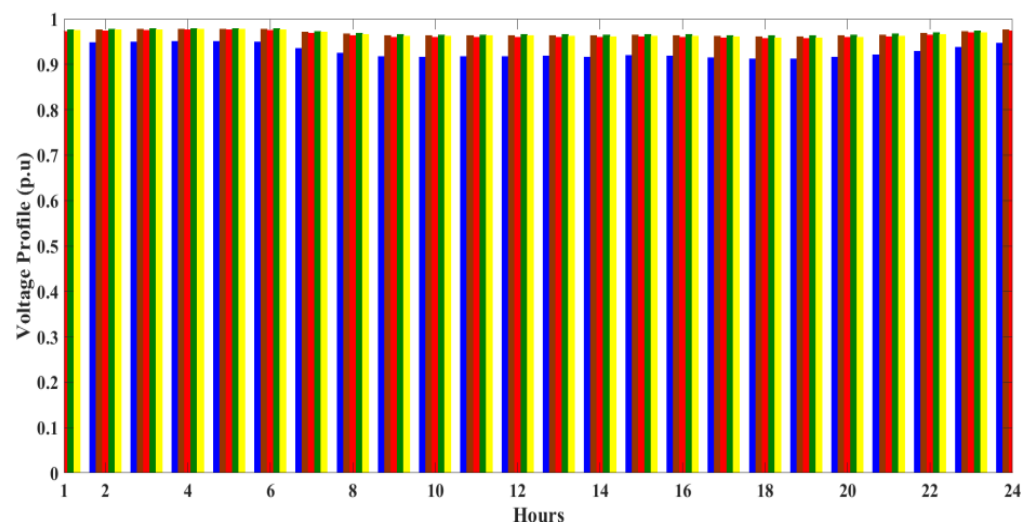


Figure 14. Voltage Profile characteristic for a typical day.

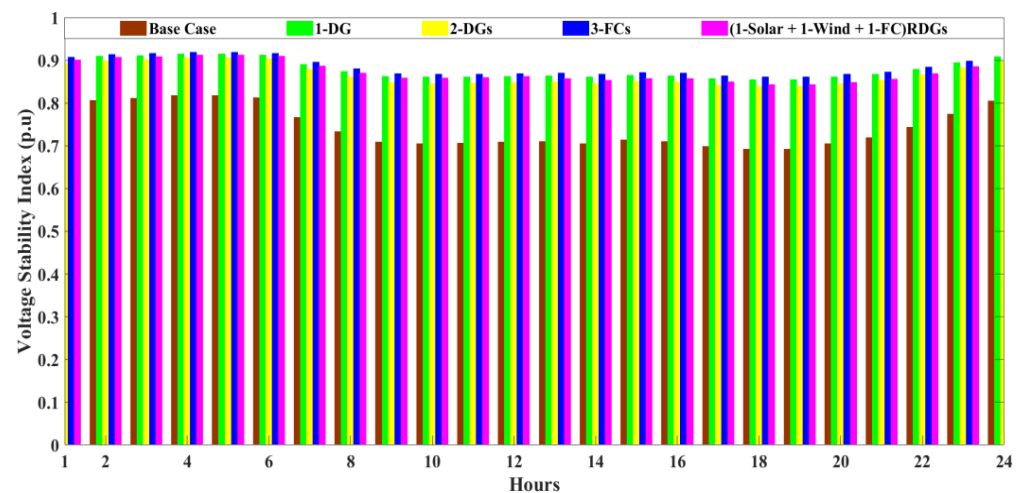


Figure 15. Voltage stability Index characteristic for a typical day.

### 5.2. Optimal Renewable-Based DGs $P_{Loss}$ for a Typical Day without EVs

The output power of RDGs is not consistent, so the 5% underestimation is taken into account and the results are tabulated in Table 6. Different cases are considered such as  $P_{Loss}$  typical day with 1-solar + 1-wind + 1-Fuel cell, 1-solar + 2-FC, 1-wind + 2-FC and 3-FCs and same represented in Figure 16. Further, the underestimation and over estimation are presented in Figures 17 and 18. Finally, RDGs are considered, along with the FC, to act as a backup source, even though RDGs do not produce the estimated power that is supplied by  $DG_3$ , such as fuel cell. Multiple case studies with and without RDGs in the DS

are taken. In addition, the findings of a thorough study performed at the peak hour (18 h) of a day are shown below. The active  $P_{Loss}$  achieved in the primary case is 68.8189 kW, and the  $V_{min}$  and  $VSI_{min}$  obtained are 0.9123 p.u, 0.6927 p.u. The VSI determines the best position for the RDGs, and the POA method determines the best size. 3-RDGs with capacities of 334.2414 kW, 230.5464 kW, and 145.6437 kW are located on the 7th, 12th, and 22nd buses. The active  $P_{Loss}$  is decreased to 33.6501 kW once the RDGs is installed, and the  $V_{min}$  and  $VSI_{min}$  are improved to 0.9633 p.u and 0.8611 p.u. Compared to the base case, 1-solar + 1-wind + 1-Fuel cell, 1-solar + 2-FC, 1-wind + 2-FC and 3-FCs case reduced 50.25%  $P_{Loss}$ ; this is illustrated in Figure 16 and the results are tabulated in Table 7.

**Table 6.** RDG and EV scheduling with considering uncertainties.

Hour	RDG <sub>1</sub> (kW)	RDG <sub>2</sub> (kW)	RDG <sub>3</sub> (kW)	CCM EVs Size (kW)	OCM EVs Size (kW)
1	0	168.6979	275.711	0	0
2	0	158.0734	258.6207	0	0
3	0	137.9663	257.2959	0	0
4	0	132.3059	247.9305	0	164.9124 93.6902 84.4630 164.8767
5	0	122.8699	251.5886	0	93.6953 84.5098 171.0092
6	23.0397	111.9504	244.8535	0	97.8715 87.0779
7	36.7313	142.016	301.0115	0	0
8	58.2045	141.6904	344.1369	0	0
9	75.3447	159.4687	366.7543	0	0
10	90.6312	194.2686	345.965	0	0
11	89.5447	216.6312	337.0031	0	0
12	94.1047	232.4594	322.7771	0	0
13	47.0657	143.4683	393.0898	0	0
14	45.1035	95.7511	423.6257	0	0
15	46.5414	105.5039	401.988	0	0
16	38.4655	136.6521	403.009	0	0
17	20.2208	142.6663	439.822	0	0
18	0	69.5131	495.9151	309.0081 193.6312 145.6272 308.9711	0
19	0	53.5084	502.79	193.6310 145.6605 293.8829	0
20	0	16.3767	493.297	183.0712 139.3334	0
21	0	23.4579	465.6374	0	0
22	0	29.9008	418.8243	0	0
23	0	42.4956	357.8433	0	0
24	0	64.0545	296.7647	0	0

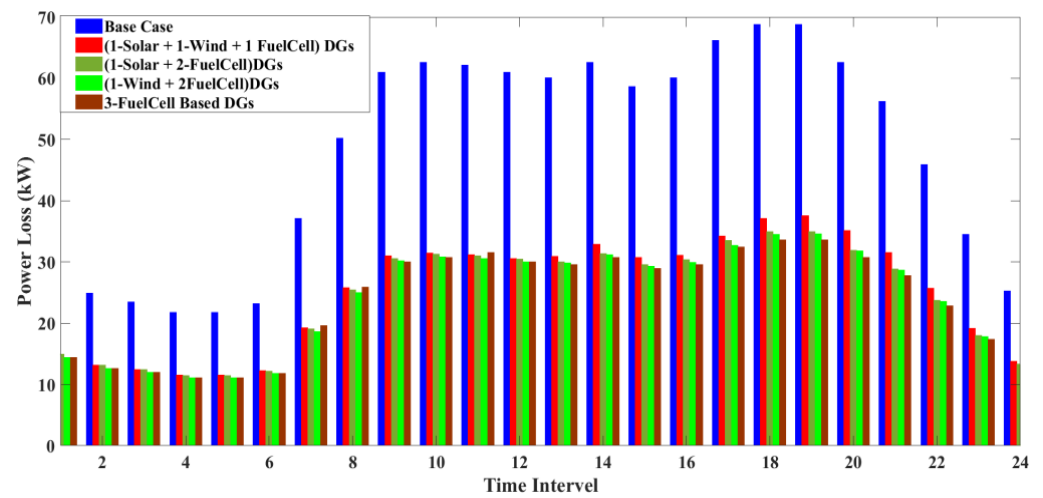


Figure 16. 28 practical test system  $P_{Loss}$  typical day with different cases.

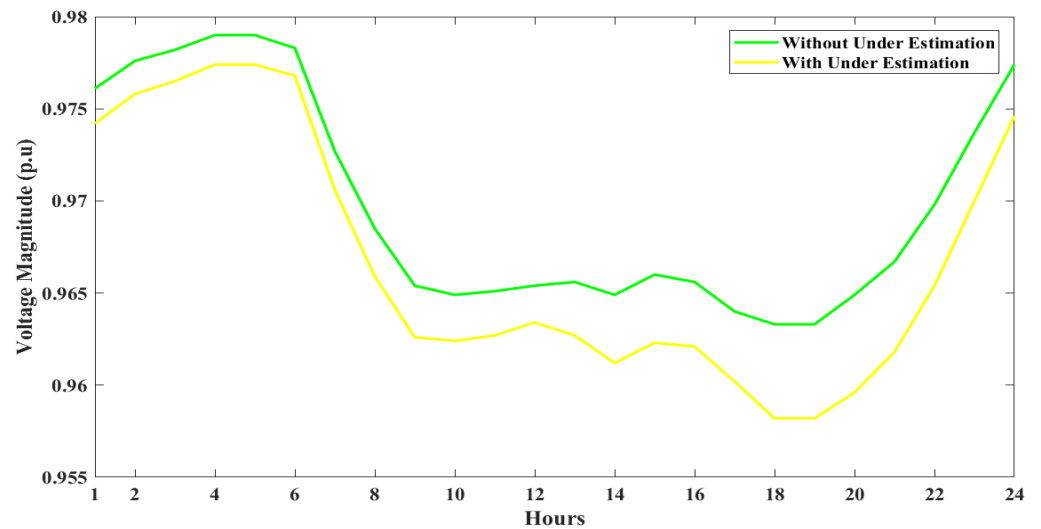


Figure 17. Voltage profile characteristic comparison with and without underestimation.

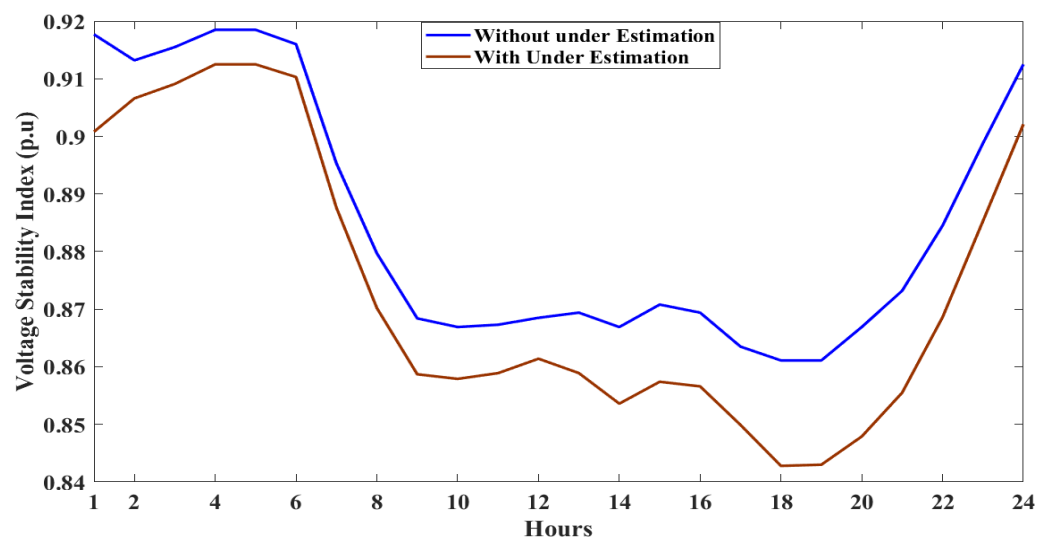


Figure 18. Voltage stability index characteristic comparison with and without underestimation.

**Table 7.** RDGs  $P_{Loss}$  comparison for a typical day with different cases.

Hours	Base Case $P_{Loss}$ (kW)	(1-Solar + 1-Wind + 1-FC) DG $P_{Loss}$ (KW)	(1-Solar + 2- FC) DGs $P_{Loss}$ (kW)	(1-Wind + 2-FC) DGs $P_{Loss}$ (kW)	3-FC Based DGs $P_{Loss}$ (kW)
1	28.4096	14.8999	14.8999	14.3656	14.3654
2	24.9163	13.1132	13.1132	12.6471	12.6454
3	23.5076	12.4037	12.3899	11.9522	11.949
4	21.751	11.4991	11.4855	11.082	11.0781
5	21.751	11.5209	11.4855	11.0936	11.0781
6	23.1827	12.21	12.1192	11.8086	11.7881
7	37.1053	19.2422	19.057	18.6662	19.6057
8	50.1845	25.8305	25.4155	25.0255	25.8845
9	61.0107	31.0461	30.5826	30.1852	30.0013
10	62.5568	31.4642	31.2581	30.8709	30.7265
11	62.1329	31.1711	31.0124	30.6008	31.5278
12	61.0107	30.5748	30.4865	30.0558	30.0013
13	60.0386	30.9146	30.0495	29.8682	29.5446
14	62.5568	32.9205	31.3512	31.1937	30.7265
15	58.6655	30.7236	29.5805	29.3434	28.8987
16	60.0386	31.0588	30.3959	29.9069	29.5446
17	66.1549	34.2544	33.5202	32.6922	32.409
18	68.8189	37.1484	34.9673	34.4751	33.6501
19	68.8189	37.5329	34.9673	34.553	33.6501
20	62.5568	35.148	31.9214	31.8015	30.7265
21	56.2403	31.5144	28.8271	28.6619	27.7552
22	45.9301	25.717	23.7262	23.5273	22.8544
23	34.5317	19.2026	18.0085	17.7884	17.3566
24	25.2543	13.8061	13.2865	13.0294	12.8123
Total $P_{Loss}$	1147.1245	604.917	583.9069	575.1945	570.5798

### 5.3. 28 Indian Real Test System Evaluation with EVs

The advantages of placing RDGs in three different modes of operation are discussed in further detail, and the expansion of scheduling EVs is further examined.

The network's operational conditions deteriorate due to the dynamic variations in system demand and the growing adaption of EVs. Consequently, EVs must be scheduled in accordance with the changing levels of demand. The Chevy Volt EV, a well-known vehicle on the market, is used as an example in this study. Table 1 lists the EV's parameters.

- There are 60 EVs that ride to work, covering an average daily distance of 30 km, departing at 8:00 a.m. and arriving back at 5:00 p.m.
- All EVs must begin their journey with a full charge, and there is no way to recharge between the hours of travel. Furthermore, EVs require significant time to charge their batteries depending on the distance travelled/supplied to the grid.
- The technology is also expected to provide a two-way communication system between EVs and the power grid. This channel permits information between them, allowing for combined EV and DG scheduling. As a result, data are transported without delay from one channel to the next.

#### 5.3.1. Conventional Charging Method (CCM)

In the CCM, EVs are recharged ideally at the 2nd, 5th, and 11th nodes. The VSI approach is used to identify these places. As illustrated in Figure 19, the EVs are charged in G2V mode throughout the 18th, 19th, and 20th h. For each hour, the  $P_{Loss}$ ,  $V_{min}$ , and  $VSI_{min}$  are calculated, and the results are shown in Table 8. The voltage profile during 18–20 h is impacted due to the increased load on the network; as shown in Table 8, the 24 h  $P_{Loss}$  is 610.1480 kW.

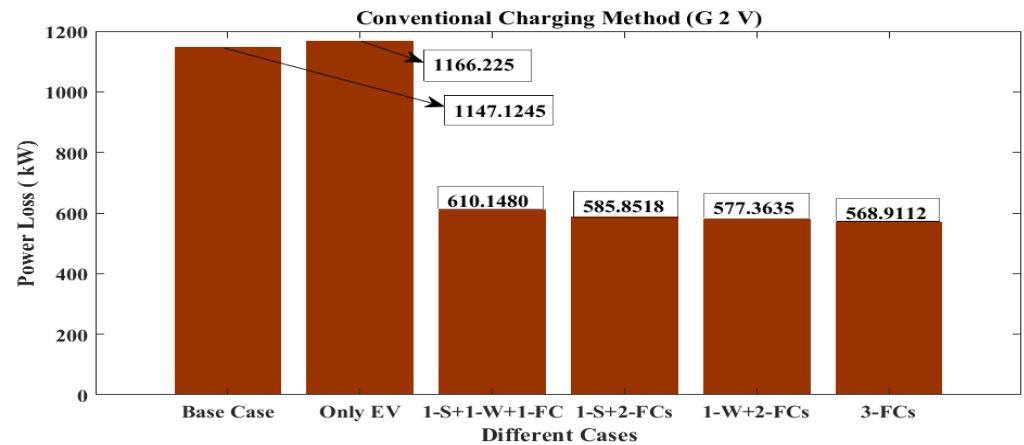


Figure 19. Conventional EV Charging method (G2V) P<sub>Loss</sub> with Different Cases.

Table 8. Comparison of P<sub>Loss</sub> for different operating conditions.

Different Cases	Total P <sub>Loss</sub> in (kW)	
Base Case	1147.1245	
Only EVs	1166.225	
Conventional EV Charging Method (G2V)	(1-S + 1-W+ 1-FC) DGs with EVs (G to V)	610.1480
	(1-S + 2-FC) DGs with EVs (G to V)	585.8518
	(1-W + 2-FC) DGs with EVs (G to V)	577.3635
	3-FC Based DGs with EVs (G to V)	568.9112
Optimised EV Charging Method (G2V)	Only EVs	1157.8053
	(1-S + 1-W+ 1-FC) DGs with EVs (G to V)	606.3257
	(1-S + 2-FC) DG with EVs (G to V)	584.6451
	(1-W + 2-FC) DG with EVs (G to V)	576.3496
(1-S + 1-W + 1-FC) DG EV Charging Method (G2V + V2G)	3-FC Based DGs with EVs (G to V)	567.9729
	(1-S + 1-W + 1-FC) DG EV Charging Method (G2V + V2G)	601.4159
	(1-S + 2-FC) DG EV Charging Method (G to V + V to G)	582.1144
	(1-W + 2-FC) DG EV Charging Method (G to V + V to G)	574.1536
(3-FC) DGs EV Charging Method (G to V + V to G)	565.6587	

### 5.3.2. Optimized Charging Method (OCM)

The OCM technology takes into account system power demand and calculates the appropriate time to charge the EVs. In an OCM, EVs are optimally located on the 2nd, 5th, and 11th buses. VSI is used to find these places. The EVs are charged in G2V mode between the 4th, 5th, and 6th h, as illustrated in Figure 20. For each hour, the P<sub>Loss</sub>, V<sub>min</sub>, and VSI<sub>min</sub> are calculated, and the results are shown in Table 8. Compared to the CCM approach, the total P<sub>Loss</sub> per day is 606.3257 kW, which is reduced. The voltage profile has been enhanced and is now superior to the CCM approach.

### 5.3.3. G2V + V2G Method

The assessment is carried out in combination with the OCM. This method allows EVs to charge and send electricity back to the grid (V2G + G2V)). The OCM approach takes into account system load demand and calculates the best time to charge the EVs. As illustrated in Figures 21 and 22, the EVs are then charged in G2V mode between the 4th and 5th h. Between the 18th and 19th h, the EVs will deliver electricity to the grid. For each hour, the P<sub>Loss</sub>, V<sub>min</sub>, and VSI<sub>min</sub> are calculated, and the results are shown in Table 8. The total daily P<sub>Loss</sub> is 601.4159 kW. Table 8 contains a comparison of several cases. The voltage profile is considerably better than with the previous approaches. Efficient EV scheduling, combined with appropriate allocation of RDGs, assists in loss minimization and improves the voltage profile.

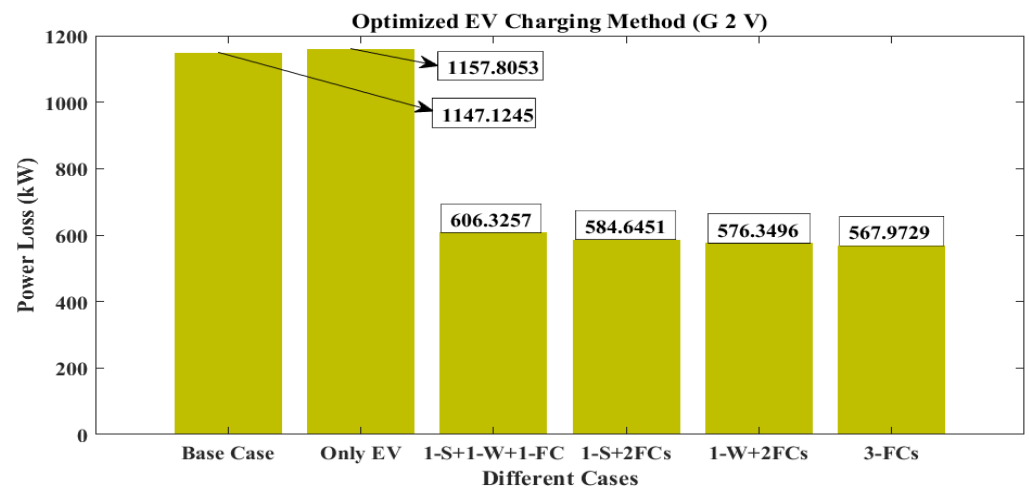


Figure 20. Optimized EV Charging method (G2V)  $P_{Loss}$  with Different Cases.

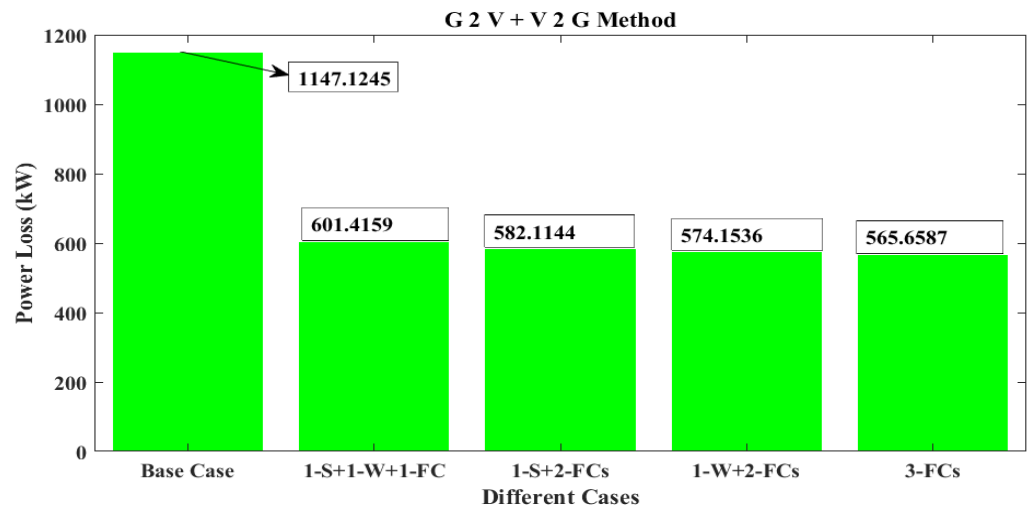


Figure 21. G2V + V2G  $P_{Loss}$  with Different Cases.

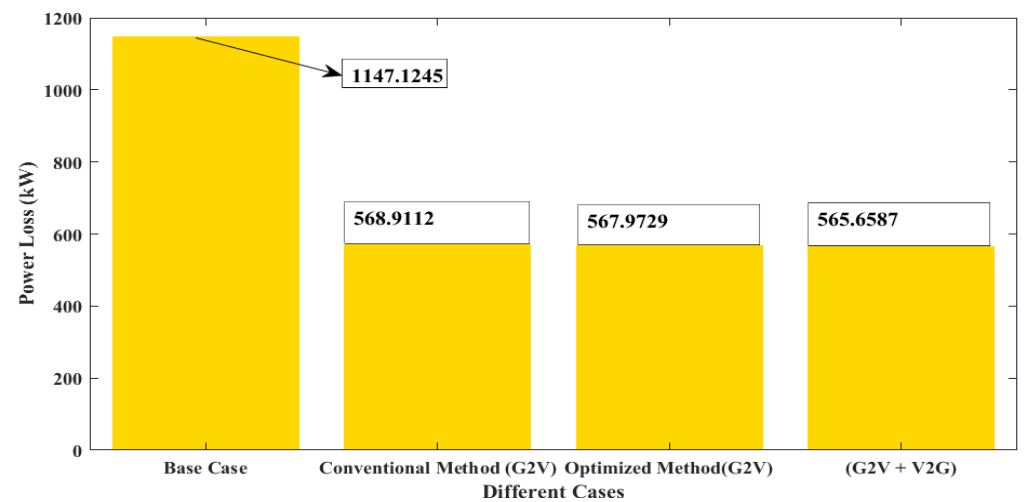


Figure 22. Compared  $P_{Loss}$  with conventional, optimized EV charging method and G2V + V2G.

## 6. Conclusions

The presented method aims to achieve minimal  $P_{Loss}$  and a better voltage profile with optimal allocation of RDGs and scheduling EVs in DS. The combination of the VSI-POA

method is proposed to find the optimal location to install RDGs and charging EVs locations and determine the size of RDGs. The proposed VSI-POA analysis was performed on 28 Indian real test systems. Compared to POA performance with other existing methods, POA gives better results with less iteration. Simultaneous allocation of RDGs with EVCS enhanced the voltage profile and reduced RES uncertainty in DS compared to a single allocation system. CCM (G2V + V2G) and OCM (G2V + V2G) implemented OCM further reduces  $P_{Loss}$ . It was observed that comparing (1-Solar + 1-wind + 1-SOFC) (G2V + V2G) 1-solar with 2-SOFC (G2V + V2G) and 1-wind with 2-SOFC (V2G + G2V) and 3-SOFC (G2V + V2G) reduces  $P_{Loss}$  and enhances the voltage profile.

**Author Contributions:** Conceptualization, N.D., S.K.S. and S.V.; methodology, N.D., S.K.S., S.V.; software, N.D., S.K.S., S.V., S.M., N.K.S., M.B., E.E., M.S. and S.K.; validation, N.D., S.K.S., S.V., S.M., N.K.S., M.B., E.E., M.S. and S.K.; formal analysis, N.D., S.K.S. and S.V.; investigation, N.D., S.K.S. and S.V.; resources, N.D., S.K.S., S.V., S.M., N.K.S., M.B., E.E., M.S. and S.K.; data curation, N.D., S.K.S. and S.V.; writing—original draft preparation, N.D., S.K.S. and S.V.; writing—review and editing, N.D., S.K.S., S.V., S.M., N.K.S., M.B., E.E., M.S. and S.K.; visualization, N.D., S.K.S., S.V., S.M., N.K.S., M.B., E.E., M.S. and S.K.; supervision, S.K.S. and S.V.; project administration, N.D., S.K.S., S.V., S.M., N.K.S., M.B., E.E., M.S. and S.K.; funding acquisition, E.E. and M.S. All authors have read and agreed to the published version of the manuscript.

**Funding:** This research received no external funding.

**Institutional Review Board Statement:** Not Applicable.

**Informed Consent Statement:** Not Applicable.

**Data Availability Statement:** Not Applicable.

**Conflicts of Interest:** The authors declare no conflict of interest.

## Nomenclature

RDGs	Renewable Distributed Generators
DS	Distribution System
$P_{Loss}$	Power Loss
PDF	Probability Distribution Function
VSI	Voltage Stability Index
POA	Political Optimizer Algorithm
CCM	Conventional Charging Method
OCM	Optimized Charging Method
DGs	Distributed Generators
EVs	Electric Vehicle
PEVs	Plug in Electric Vehicles
MG	Micro Grids
EVCS	Electric Vehicle Charging Station
RES	Renewable Energy Resources
DERs	Distributed Energy Resources
SOFC	Solid Oxide Fuel Cell
PEMFC	Proton Exchange Membrane Fuel Cell
PV	Photo Voltaic
WT	Wind Turbine
PDF	Probability Distribution Function
FC	Fuel Cell
SoC	State of Charge
DoC	Decision on Charge
PAR	Peak-to0Average Ratio
$P_R$	Power Ratio
G2V	Grid 2 Vehicle
V2G	Vehicle 2 Grid

$P^{FC}$	Fuel Cell output power
$E^{FC}_o$	Potential Difference
$I^{FC}$	Current Flow
$R^{FC}$	FC Electrodes have an internal resistance b/w them
$A^{FC}$	FC Electrode Surface Area
$R, r$	Global Gas Constant (J/mol k), internal Resistance (ohm)
$T$	Temperature (kelvin)
$pH_2, pO_2, pH_2O$	Hydrogen, Oxygen and Water (atm)
$N^0, E^0$	No. of Cells, Reversible Cell (volts)
$f_s^m(s)$	Beta PDF for Solar Irradiance
$\alpha^m, \beta^m$	Shape Parameters
FF	Fill Factor
$N^{PVM}$	Total Number of PV modules
$I_{sc}$	Short Circuit Current
$V_{oc}$	Open Circuit Voltage
$T^{cy}$	Cell Temperature
$T^A$	Ambient Temperature
$K^i, K^v$	Current & Voltage Temperature Coefficients
$N^{OT}$	Nominal Operating Temperature
$f_v(V)$	Weibull PDF for Wind Speed
$k$	Shape Factor
$c$	Scale Factor
$P_{WE}$	Expected Output Power of Wind Turbine

## References

1. Shaheen, A.; Elsayed, A.; Ginidi, A.; El-Sehiemy, R.; Elattar, E. Improved Heap-Based Optimizer for DG Allocation in Reconfigured Radial Feeder Distribution Systems. *IEEE Syst. J.* **2022**, 1–10. [\[CrossRef\]](#)
2. Taha, H.A.; Alham, M.H.; Youssef, H.K.M. Multi-Objective Optimization for Optimal Allocation and Coordination of Wind and Solar DGs, BESSs and Capacitors in Presence of Demand Response. *IEEE Access* **2022**, *10*, 16225–16241. [\[CrossRef\]](#)
3. Suresh, V.; Pachauri, N.; Vigneysh, T. Decentralized control strategy for fuel cell/PV/BESS based microgrid using modified fractional order PI controller. *Int. J. Hydrog. Energy* **2021**, *46*, 4417–4436. [\[CrossRef\]](#)
4. Farrokhhabadi, M.; Lagos, D.; Wies, R.W.; Paolone, M.; Liserre, M.; Meegahapola, L. Microgrid Stability Definitions, Analysis, and Examples. *IEEE Trans. Power Syst.* **2020**, *35*, 13–29. [\[CrossRef\]](#)
5. Padhi, P.P.; Nimje, A.A. Distributed Generation: An Overview. *Int. Electr. Eng. J.* **2012**, *3*, 607–611.
6. Rama Prabha, D.; Jayabarathi, T.; Umamageswari, R.; Saranya, S. Optimal location and sizing of distributed generation unit using intelligent water drop algorithm. *Sustain. Energy Technol. Assess.* **2015**, *11*, 106–113. [\[CrossRef\]](#)
7. Sanjay, R.; Jayabarathi, T.; Raghunathan, T.; Ramesh, V.; Mithulananthan, N. Optimal allocation of distributed generation using hybrid grey Wolf optimizer. *IEEE Access* **2017**, *5*, 14807–14818. [\[CrossRef\]](#)
8. Uniyal, A.; Sarangi, S. Optimal network reconfiguration and DG allocation using adaptive modified whale optimization algorithm considering probabilistic load flow. *Electr. Power Syst. Res.* **2021**, *192*, 106909. [\[CrossRef\]](#)
9. Huy, T.H.B.; Tran TVan Ngoc Vo, D.; Nguyen, H.T.T. An improved metaheuristic method for simultaneous network reconfiguration and distributed generation allocation. *Alexandria Eng. J.* **2022**, *61*, 8069–8088. [\[CrossRef\]](#)
10. Shaheen, A.; Elsayed, A.; Ginidi, A.; El-Sehiemy, R.; Elattar, E. Reconfiguration of electrical distribution network-based DG and capacitors allocations using artificial ecosystem optimizer: Practical case study. *Alexandria Eng. J.* **2022**, *61*, 6105–6118. [\[CrossRef\]](#)
11. Kayal, P.; Chanda, C.K. Optimal mix of solar and wind distributed generations considering performance improvement of electrical distribution network. *Renew Energy* **2015**, *75*, 173–186. [\[CrossRef\]](#)
12. Home-Ortiz, J.M.; Pourakbari-Kasmaei, M.; Lehtonen, M.; Sanches Mantovani, J.R. Optimal location-allocation of storage devices and renewable-based DG in distribution systems. *Electr. Power Syst. Res.* **2019**, *172*, 11–21. [\[CrossRef\]](#)
13. Jafar-Nowdeh, A.; Babanezhad, M.; Arabi-Nowdeh, S.; Naderipour, A.; Kamyab, H.; Abdul-Malek, Z.; Ramachandaramurthy, V.K. Meta-heuristic matrix moth–flame algorithm for optimal reconfiguration of distribution networks and placement of solar and wind renewable sources considering reliability. *Environ. Technol. Innov.* **2020**, *20*, 101118. [\[CrossRef\]](#)
14. Rathore, A.; Patidar, N.P. Optimal sizing and allocation of renewable based distribution generation with gravity energy storage considering stochastic nature using particle swarm optimization in radial distribution network. *J. Energy Storage* **2021**, *35*, 102282. [\[CrossRef\]](#)
15. Hassan, A.S.; Sun, Y.; Wang, Z. Water, Energy and Food Algorithm with Optimal Allocation and Sizing of Renewable Distributed Generation for Power Loss Minimization in Distribution Systems (WEF). *Energies* **2022**, *15*, 2242. [\[CrossRef\]](#)



16. Liu, J.P.; Zhang, T.X.; Zhu, J.; Ma, T.N. Allocation optimization of electric vehicle charging station (EVCS) considering with charging satisfaction and distributed renewables integration. *Energy* **2018**, *164*, 560–574. [[CrossRef](#)]
17. Hariri, A.M.; Hejazi, M.A.; Hashemi-Dezaki, H. Reliability optimization of smart grid based on optimal allocation of protective devices, distributed energy resources, and electric vehicle/plug-in hybrid electric vehicle charging stations. *J. Power Sour.* **2019**, *436*, 226824. [[CrossRef](#)]
18. Gupta, K.; Achathuparambil Narayanankutty, R.; Sundaramoorthy, K.; Sankar, A. Optimal location identification for aggregated charging of electric vehicles in solar photovoltaic powered microgrids with reduced distribution losses. In *Energy Sources, Part A: Recovery, Utilization and Environmental Effects*; Taylor & Francis: Oxfordshire, UK, 2020; pp. 1–16.
19. Pal, A.; Bhattacharya, A.; Chakraborty, A.K. Allocation of electric vehicle charging station considering uncertainties. *Sustain. Energy Grids Netw.* **2021**, *25*, 100422. [[CrossRef](#)]
20. Li, C.; Zhang, L.; Ou, Z.; Wang, Q.; Zhou, D.; Ma, J. Robust model of electric vehicle charging station location considering renewable energy and storage equipment. *Energy* **2022**, *238*, 121713. [[CrossRef](#)]
21. Padullés, J.; Ault, G.W.; McDonald, J.R. Integrated SOFC plant dynamic model for power systems simulation. *J. Power Sources* **2000**, *86*, 495–500. [[CrossRef](#)]
22. Lavorante, M.J.; Sanguinetti, A.R.; Fasoli, H.J.; Aiello, R.M. Equation for General Description of Power Behaviour in Fuel Cells. *J. Renew Energy* **2018**, *2018*, 2678050. [[CrossRef](#)]
23. Ranjan, R.; Venkatesh, B.; Das, D. Voltage stability analysis of radial distribution networks. *Electr. Power Compon. Syst.* **2003**, *31*, 501–511. [[CrossRef](#)]
24. Borji, A. A new global optimization algorithm inspired by parliamentary political competitions. In *Lecture Notes in Computer Science; including Subser Lecture Notes Artificial Intelligence Lecture Notes Bioinformatics*; Springer: Berlin, Germany, 2007; pp. 61–71.
25. Askari, Q.; Younas, I.; Saeed, M. Political Optimizer: A novel socio-inspired meta-heuristic for global optimization. *Knowl. Based Syst.* **2020**, *195*, 105709. [[CrossRef](#)]
26. Zhu, A.; Gu, Z.; Hu, C.; Niu, J.; Xu, C.; Li, Z. Political optimizer with interpolation strategy for global optimization. *PLoS ONE* **2021**, *16*, e0251204.